SAND2013-3013C
Proceedings of ASME 2013 International Mechanical Engineering Congress & Exposition
IMECE2013
November 15-21, 2013, San Diego, CA, USA

IMECE2013-63270

DRAFT: AN EXPLORATION OF ACCURACY AND CONVERGENCE OF THE DEGENERATE UNIFORM STRAIN HEXAHEDRAL ELEMENT (A SOLUTION TO THE UNMESHED VOID IN AN ALL-HEXAHEDRAL MESH)

Timothy R. Shelton*
Sandia National Laboratories
PO Box 5800, MS 0380
Albuquerque, NM 87185
Email: trshelt@sandia.gov

Nathan K. Crane
Sandia National Laboratories
PO Box 5800, MS 0380
Albuquerque, NM 87185

James V. Cox
Sandia National Laboratories
PO Box 5800, MS 0380
Albuquerque, NM 87185

ABSTRACT

The uniform strain hexahedral element mesh has long been a work horse for getting accurate and convergent answers in high deformation solid mechanics analyses. Obtaining an all-hexahedral mesh can be difficult and time consuming process and this has severely limited the element's use in design phase computations. Unconstrained paving and plastering offers a technique to get an all-hexahedral mesh automatically but still can leave un-meshable voids [1]. While degenerated forms of the uniform strain hexahedral element such as the wedge have been used sparingly, they have garnered limited general acceptance. We present a more exhaustive numerical exploration of the degenerated hexes with the hope of encouraging their use to resolve the un-meshable voids. The results of patch tests are used to numerically demonstrate linear completeness of the degenerate elements. A manufactured solution analysis is then used to show optimal convergence rates for meshes containing degenerate elements. Additionally, applications to a torsion bar and high velocity impact are used to highlight the accuracy and applicability of degenerates for solving more complex problems.

INTRODUCTION

Estimates are that model setup make up the majority (80%) of the time in a modeling and simulation work flow [2]. Of the setup time, an obvious place for speed up is through automation in the meshing of geometry. All-tetrahedral meshing has been successful at allowing fast meshing. However, all-tetrahedral meshes are inefficient for many solid mechanics applications. Hexahedral meshes are desired for their improved accuracy at lower fidelity which translates to faster turn around time.

There have been many attempts at accomplishing an automated all-hexahedral mesh. Attempts like that presented in the paper "Unconstrained Paving and Plastering: A New Idea for All Hexahedral Meshing" are able to mesh the vast majority of a complex domain, but may still encounter small un-meshable voids [1]. These un-meshable voids arise from the constraints that are required to get an all-hexahedral mesh [3]. Relaxing these constraints by allowing some additional element shapes can lead to further automation of the mesh creation process [4].

In this paper we explore the versatility of the uniform strain hexahedral to support a family of different element shapes and topologies. We will try and alleviate some of the fear behind using these sub-shapes of the hexahedral by showing that they are convergent and compare favorably with the accuracy of an all-hexahedral mesh.

FAMILY OF DEGENERATES

There are numerous polyhedral shapes that can be made with four to eight nodal vertexes. If we limit the shapes to be derived by collapsing the node of an eight node hexahedral shape then we get to a manageable set and gain some advantages over starting from an arbitrary point cloud. The main advantage of collapsing nodes in the hexahedral shape is that all the shapes can fit in the

*Address all correspondence to this author.

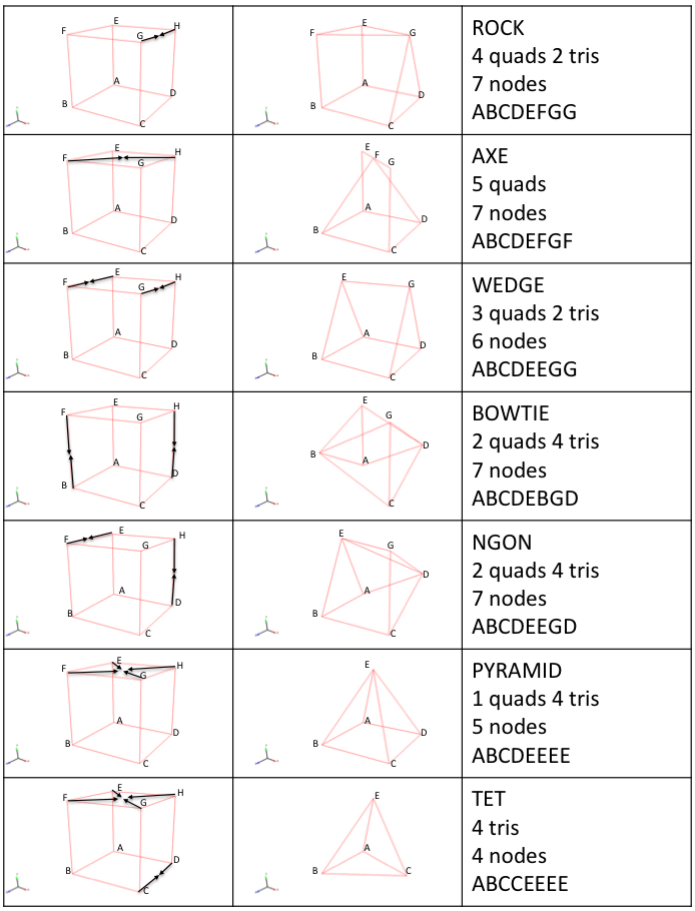

FIGURE 1. HEXAHEDRAL DEGENERATE ELEMENT FAMILY.

same connectivity table by simply allowing repeated node IDs. This repeated node connectivity may then be processed directly by the same element numeric implementation that processes the standard eight node hexahedral element.

Since the hexahedral shape is constructed from six quadrilateral faces, the sub-shapes generated from collapsing points will result in some combination of quadrilateral and triangular faces. Quadrilateral and triangular faces are the norm in most finite element simulations and as such are supported for features like contact and exact pressure integration. The polygon faces above quadrilateral do not have as wide spread support. With an eye toward being able to use the elements with features such as contact, an additional requirement is added: that nodes not be collapsed across the body diagonals because the resulting shapes would almost always have severely warped faces. This leaves the set of polyhedral shapes shown in Figure 1.

Repeating node IDs in the hexahedral connectivity is commonly referred to as a *degenerate hex*. The wedge, pyramid, and

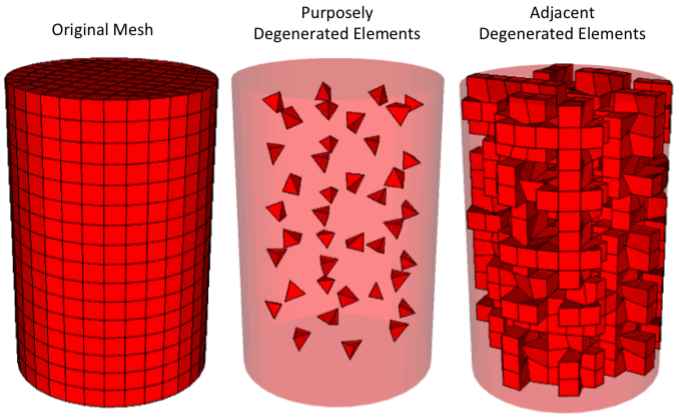

FIGURE 2. DEGENERATE ELEMENT INSERTION

tetrahedral degenerated forms sometimes have their own unique element formulations but, as shown in this paper, can run also through the same computational machinery as the uniform strain hexahedral.

DEGENERATE INSERTION

Most current meshing software avoids inserting degenerate elements. If degenerate elements are created during meshing they will often error out, not returning any mesh. It was necessary to write a tool for insertion of degenerates in an existing all-hexahedral mesh to enable these elements to be studied. The degeneration insertion algorithm first marks elements that do not share any neighbors. The marked elements are then purposely degenerated to a target degenerate shape with a random orientation. Figure 2 shows the torsion bar mesh for h = 0.25 degenerated to insert thirty nine tetrahedral degenerate hexes. Degenerating a hexahedral element in an existing mesh causes some of its neighbors to also become degenerates. These incidentally degenerated elements are also shown in Figure 2. Ultimately about 25% of the elements in the Hex/Tet torsion bar mesh have been converted to some degenerate form.

UNIFORM STRAIN HEXAHEDRON

In this study the eight node uniform strain hexahedron element is used [5]. When coupled with hourglass mode control this under-integrated brick element has proven to be very efficent, accurate, and versatile. The uniform strain hexahedron element is a workhorse element for most implicit and explicit solid mechanics computations done with the Sierra Solid Mechanics code [6].

The Sierra Solid Mechanics code was used exclusively in this study for all the simulation calculations. No additional code machinery was added to Sierra to handle the degenerate hexahedral elements either for strain computations or hourglass resistances. The degenerate elements are formed by simply repeating nodes in the element connectivity in the mesh file.

MEASURING UP

In order for the degenerated hexahedral elements to be accepted as part of a mesh it has to be shown that their presence will not destroy the accuracy or degrade the convergence of an analysis. The most common competition for the all-hexahedral mesh is the all-tetrahedral mesh so, when appropriate, comparisons are made to the standard tetrahedral formulation. Also, given that these problems are numerical examples and not meant for physical interpretation, units are absent since any consistent set of units could be applied to the numbers presented.

PATCH TEST

Generally, the first thing a new element is tested with is a patch test. The patch demonstrates that an element can exactly represent a known constant stress/strain solution. Viewing each degenerate case of the uniform strain hexahedral element as a new element, a patch test was performed for each possible degenerate shape, serving as the middle element. A version of the patch test described in the Sierra/SM Verification Tests Manual [7] was modified to test each degenerate element shape. This patch test ensures that the element can represent a constant field exactly without the element having any special shape or alignment to the field.

The center element in the patch was degenerated by merging node ID pairs to form a center element with all possible node pairings. The merging of node 1 into node 2 was considered different than node 2 into node 1 as it gives a different orientation of the element and is represented by a different element connectivity array. Figure 3 shows the starting configuration of the original hexahedral mesh and a degeneration of the hexahedral mesh for merging node 8 into node 7.

The resulting node pairings while eliminating body diagonal pairings gave 1824 different configurations to test. All versions of the test passed the patch test with the same numerical error as the non-degenerated patch test, a numerical error of roughly 1.0e-12 in the stress resultant for a known applied strain on an elastic material.

MANUFACTURED QUADRATIC FIELD

After passing the initial patch test, a more complicated element verification test was performed with all the degenerate forms. In this element test the convergence rate is examined to determine how well the degenerated meshes can represent a simple quadratic displacement field over a cube with coordinates varying from -1 to 1.

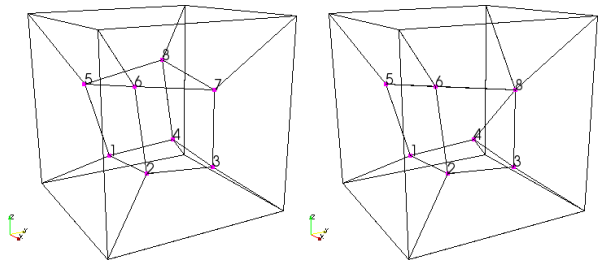

(a) ORIGINAL HEXAHEDRAL PATCH MESH (b) EXAMPLE DEGENERATED HEXAHEDRAL PATCH MESH

FIGURE 3. HEXAHEDRAL PATCH MESH ALTERATIONS

The procedure for insertion of the degenerate elements into the original all-hexahedral mesh is shown in Figure 2. This test utilizes a simple dicing routine for mesh refinement that produces a *proper refinement* (in the sense that the approximate solution space of a coarser mesh is a subspace for finder meshes). As the mesh is diced, the volume fraction of degenerates goes down. This reduction in the volume fraction of degenerates with mesh refinement is consistent with typical meshing in that the volume fraction of sub-optimal shapes decreases with refinement.

This test uses a manufactured solution obtained using symbolic calculations in Mathematica. One can think of it as taking one step past a patch test, since the polynomial representation of the displacement field is one order higher – quadratic in the initial coordinates (X) [8]. In the most general case, a complete quadratic polynomial representation of each displacement component requires 30 arbitrary constants. The simple case presented here, only has one nonzero constant, with the displacement field given by

$$\mathbf{u_1} = \mathbf{a}\mathbf{X}_\mathbf{2}^\mathbf{2}, \mathbf{u_2} = \mathbf{0.0}, \mathbf{u_3} = \mathbf{0.0}, \tag{1}$$

where **a** has units of 1/length. Here we choose to pose the problem in terms of displacement boundary conditions alone. Figure 4 depicts the displacement boundary conditions on the cube with the shading illustrating the x-component of the displacement field.

The material model used for this problem is the St. Venant-Kirchoff model, with elastic constants of **E**=1.0e6 psi, and ν=0.3. Starting with the given displacement field, one can determine the Green strain tensor, use the St. Venant-Kirchoff model to obtain the 2nd Piola-Kirchoff stresses, determine the Cauchy stress tensor and then use equilibrium to back out the body forces, which are given by

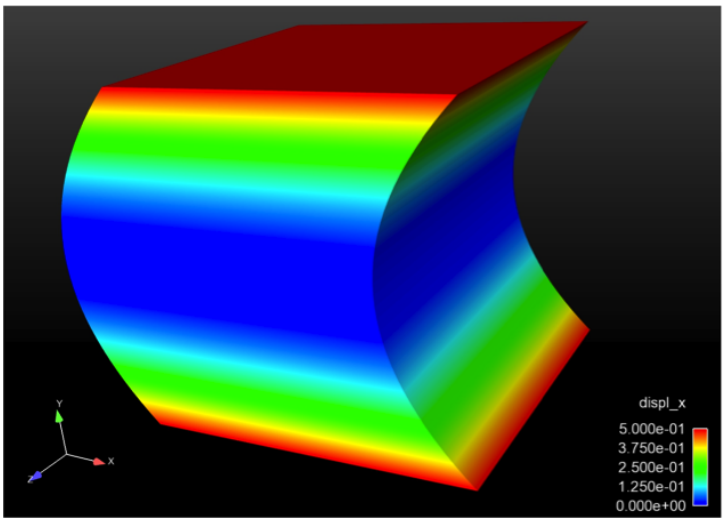

FIGURE 4. MANUFACTURED PROBLEM DISPLACEMENT FIELD

$$\mathbf{f_0} = -\mathbf{2a}[\mu + \mathbf{6a^2}(\lambda + \mathbf{2}\mu)\mathbf{X_2^2}]\mathbf{E_1} - \mathbf{4a^2}(\lambda + \mathbf{2}\mu)\mathbf{X_2}\mathbf{E_2} \quad (2)$$

where μ and λ are the Lame constants.

The symmetry in the body load vectors about the y=0 plane is consistent with the expected response. Note that these are the body loads per initial volume. It is interesting to note, in the context of evaluating elements, that the boundary value problem that is implied by the above equations, lacks any volume change independent of the shape of the domain (*i.e.*, cube or otherwise). As such this test only exercises the elements for distortional deformation.

Figure 5 shows the relative error in terms of an L2-norm of the displacement field. Note that the optimal rate of convergence, quadratic, is obtained for each degenerate element case, and that the accuracy of each case is almost identical to the non-degenerate element.

Figure 6 shows the relative error in terms of an L2-norm of Voight notation form of the stress tensor (meaning that only one of the equal, off-diagonal, symmetric terms is included in the norm calculation). Again the optimal rate of convergence (in this case linear) is obtained for each degenerate element case, with the accuracy being almost identical to the non-degenerate element.

STATIC TORSION OF ROD

After successful completion of the element tests, the degenerate element family was tested on two application oriented problems. In these application problems engineering quantities of in-

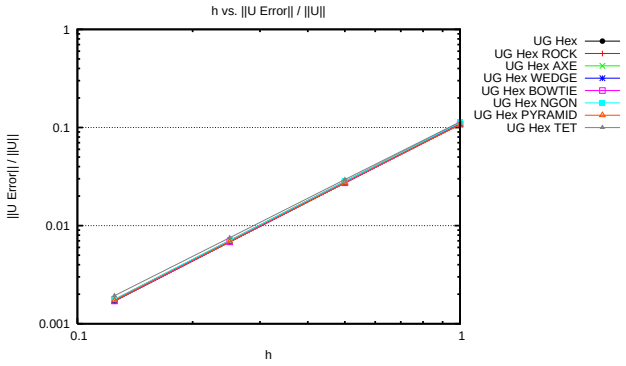

FIGURE 5. MANUFACTURED PROBLEM DISPLACEMENT FIELD CONVERGENCE PLOT

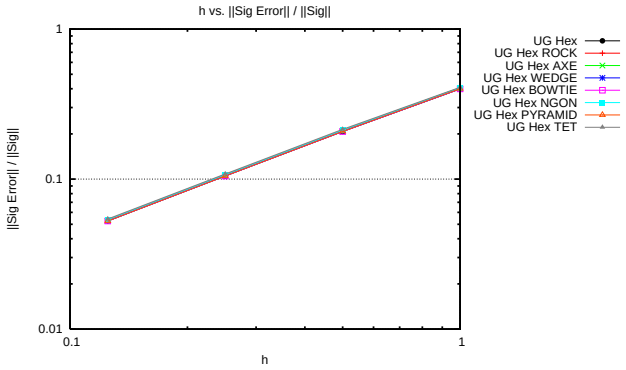

FIGURE 6. MANUFACTURED PROBLEM STRESS FIELD CONVERGENCE PLOT

terest provided by the finite element analysis are examined for accuracy as well as convergence. The geometries of these application problems are simple enough to allow straight forward all-hex meshing. However, the same accuracy implications seen in use of degenerate elements for these problems should carry over to more complex domains where the availability of degenerate elements may ease meshing. For the purpose of examining degenerate forms of the hexahedral in a static simulation, a twisted rod simulation is performed. This simulation exercises the elements in shear, though due to Poisson's ratio a variety of mixed mode deformations will be present. An elastic cylinder with a radius of 1 and height of 3 is kinematically twisted 15 degrees to ensure the elements undergo a deformation beyond the infinitesimal deformation range that was exercised in the patch tests.

For the refinement levels, a value of h = 1 corresponds to an element edge length of 0.75. Degenerate meshes were created by using the degenerate insertion shown in Figure 2 on each refinement level of the all-hexahedral meshes rather than dicing an earlier degenerate mesh. This was done to make the test more difficult by keeping the volume fraction of degenerate elements closer to constant during refinement as opposed to decreasing with each refinement. Also, this can make the accuracy inter-

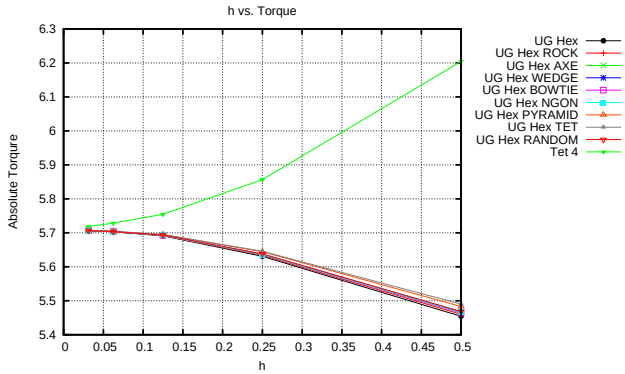

FIGURE 7. TORSION ROD TORQUE CONVERGENCE PLOT

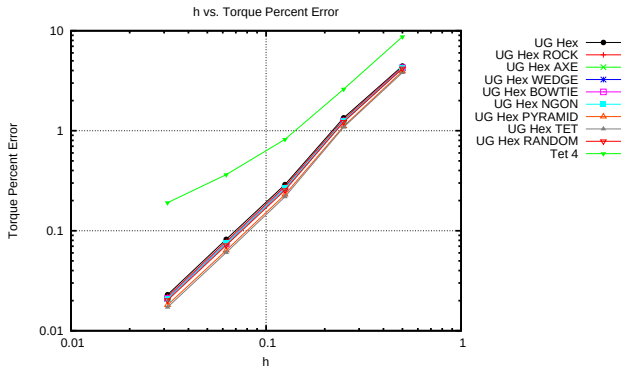

FIGURE 8. TORSION ROD TORQUE ERROR CONVERGENCE PLOT

pretation at each mesh size more relevant to a design calculation where a mesh refinement may not be possible. In addition the inserting various types of degenerate elements a final "RANDOM" mesh type is tested. In the "RANDOM" mesh types a mixed variety of all different topologies of degenerate elements are inserted.

The two engineering quantities chosen to examine in this test are the required torque and the maximum Von Mises stress. The generated torque is affected most by the approximation of the cross-sectional area, and the shear stiffness of the elements. Since for a given mesh density both hexahedral and standard tetrahedral elements have the same outer edge lengths and no mid-side nodes, their cross-sectional areas should be equivalent. Thus, the only factor affecting the results is how stiff the elements behave. The standard tetrahedral is known to be a stiffer element than the uniform strain hexahedral. This is clear in Figure 7, where the standard tetrahedral element (Tet 4) converge to the exact torque solution from the stiff side (*i.e.*, from above) and the uniform strain hexahedral (UG Hex) converges from the compliant side.

Results for the degenerate element meshes are much closer to those of the uniform strain hexahedral elements but exhibit a stiffer response in an expected pattern, as they degenerate down to a tetrahedral form (UG Hex TET). The fact that the degenerate forms are bracketed by the standard tetrahedral and the uniform strain hexahedral, combined with the two converging from above and below, serendipitously results in all the degenerate forms having a more accurate answer than the standard element. Figure 8 also shows that the slope corresponding to the convergence rate is approximately 3.5 for all the hexahedral forms, which is close to the expected slope of 4 for a quadratic convergence rate.

A contour plot of the resulting Von Mises stress for the all-hexahedral mesh with a h = 0.25 is shown in Figure 9. As expected, the maximum values appear on the outer edge of the cylinder. The maximum Von Mises stress is a more difficult test for the degenerate forms because a badly shaped element could potentially cause a spurious stress concentration, if the degenerate element appeared stiffer than the adjacent elements. Figure 10 shows the error in the infinity norm of the Von Mises stress (maximum error anywhere in the model). The degenerate forms again perform well, no spurious stress spikes are observed in the degenerate mesh solutions. The degenerate mesh stress solutions appear smooth and accurate. The slopes for stress convergence for all the mesh types are are 1.9 or larger, which is close to the expected slope of 2 corresponding to a linear convergence rate for stress. Ultimately with refinement the maximum Von Mises stress will converge to the stress at the outer cylinder surface. Some of the more aggressively degenerated mesh forms such as the Hex/Tet, Hex/Pyramid, and Random appear to show lower than expected levels of error in the stress. Possibly this lower error is due to the presence of a degenerated element moving at least one stress integration point further out radially in the cylinder in these aggressively degenerated meshes.

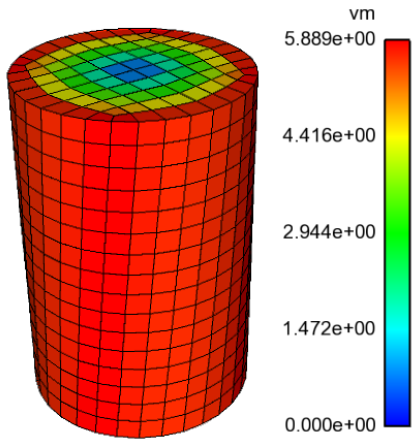

FIGURE 9. VON MISES STRESS CONTOUR PLOT OF h = 0.25 TORSION BAR

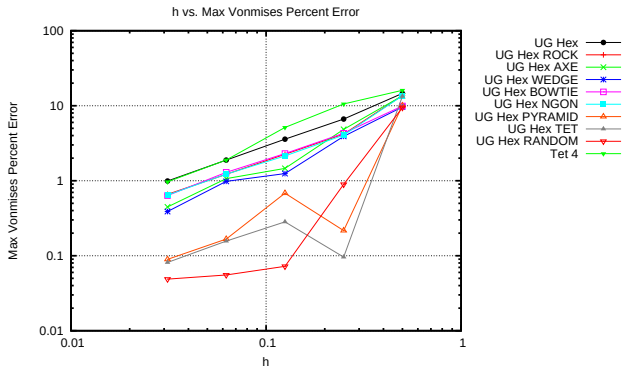

FIGURE 10. TORSION ROD MAXIMUM VON MISES ERROR CONVERGENCE PLOT

TAYLOR BAR IMPACT

A second application study of degenerate hex elements is performed based on the Taylor bar impact test. The model setup is shown in Figure 11. In the Taylor bar impact test, a cylinder of ductile material is shot against a wall at a high rate of speed. Experimentally measured deformations of the rod can be correlated to elastic plastic material properties. The Taylor bar impact test was selected to determine how well the degenerate elements perform in a dynamic problem with very large material deformation. The simulated setup is similar to a 3.3 cm long brass cylinder with an impact speed of 277 m/s. This impact velocity caused substantial deformation at the impact point, with the largest strains in the model approaching 400%. For this study we only investigated how efficiently the different mesh setups converge to the numerical solution; no comparison is made to experimental data.

Two global quantities are measured with the computational model: (1) shortening of the rod during impact, and (2) final average radius at the impacting cylinder face. Four mesh refinement levels were used to measure convergence. The coarsest mesh, h=0.25, has four elements though the bar radius and is shown in Figure 11. The "exact" solution for the problem, (i.e., reference solution) used to measure the error, was computed by using Richardson extrapolation between a h=0.03125 (the finest mesh plotted) and an even finner h=0.015625 all-hexahedral mesh solution.

Results for convergence of bar shortening and the bar end radius are shown in Figures 12 and 13. Both convergence plots show the same features. For both deformation metrics the all-hex mesh appears to be somewhat more accurate than the degenerate meshes for a given refinement level. The all-hex mesh and the various degenerate meshes appear to be converging to the exact solution at roughly the same rate. Generally it appears that the less aggressively degenerated mixed meshes, such as the "rock", perform somewhat better then meshes that contain hexes degenerated all the way to tetrahedral topologies. The accuracy of all the mixed degenerate meshes is always within a factor of

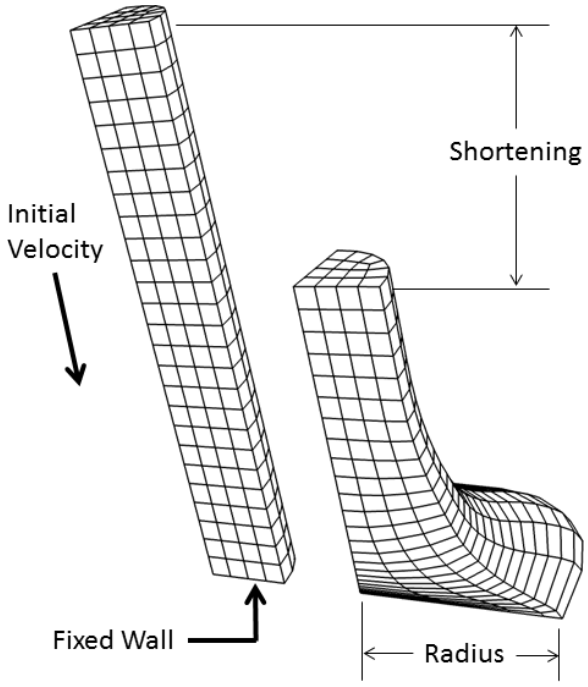

FIGURE 11. TAYLOR BAR MODEL SETUP

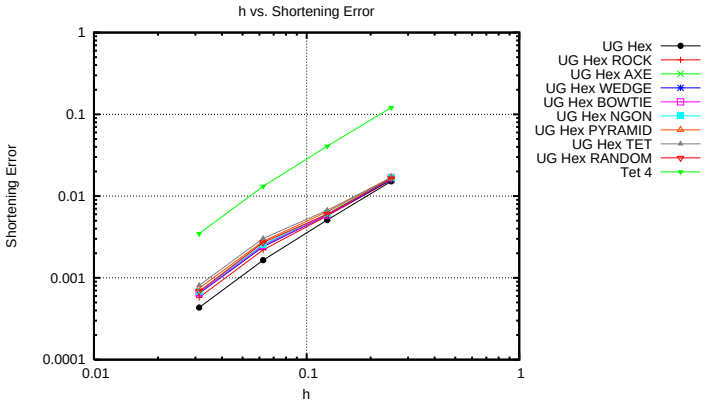

FIGURE 12. TAYLOR BAR SHORTENING CONVERGENCE

two of the all-hex mesh, while the accuracy of the all-tetrahedral mesh trails far behind either the all-hexahedral mesh or any of the mixed degenerate meshes.

For explicit dynamic computations a second important factor for efficent solution is the critical integration time step size. Table shows the explicit time steps computed on the h=0.0625 meshes. The element time step column shows the result of the element local time step computation. This element time step computation can be quickly done local to an element and produces a conservative estimate of models maximum possible explicit time step. The global time step column shows the actual system model

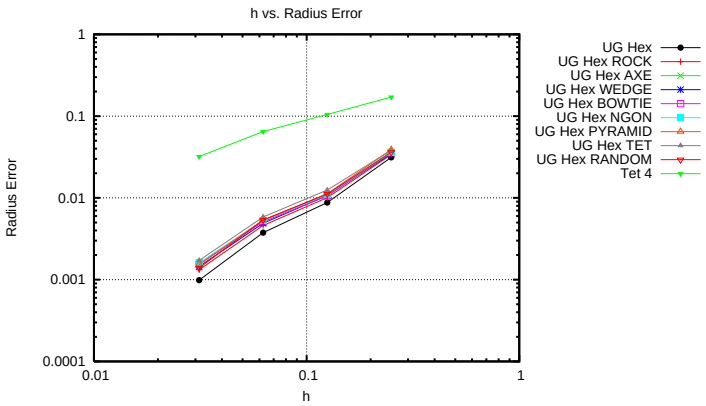

FIGURE 13. TAYLOR BAR IMPACT RADIUS CONVERGENCE

maximum critical time step as computed via computation of the maximum system stiffness matrix Eigenvalue. This global time step is the maximum explicit time step that the finite element analysis can actually take while remaining stable. A large critical time step is preferable as the larger the time step that can be taken the faster a computation can be completed.

Mesh	Computed Min Element Time Step(ns)	Actual Model Min Time Step(ns)
Hex	19.4	19.5
Hex/Rock	16.8	18.8
Hex/Ngon	16.8	17.9
Hex/Bowtie	16.8	17.8
Hex/Axe	13.3	16.8
Hex/Pyramid	13.1	16.7
Hex/Wedge	11.5	16.1
Hex/Tet	10.5	15.0
All-tet	8.0	9.1

TABLE 1. Degenerate Element Mesh Explicit Time Steps

Without any modifications to the base element formulation, the degenerate elements are able to compute a conservative element-based explicit time step. The computed time step value on the mixed degenerate meshes, tends to be more overly conservative than an all-hex mesh. This over-conservative element time step tendency is likely due to the construction of the mesh with relatively stiffer degenerate elements adjacent to somewhat softer full hex elements. The degenerate elements require a mildly smaller time step than the standard hex elements but may take larger time steps than equivalently sized all-tet meshes.

The Taylor bar results indicate that though the all-hex mesh is ideal for this problem, use of a mixed degenerate mesh incurs only a minor loss in computational solution efficiency. The accuracy of the results for all of the mixed degenerate meshes are within a factor of two of the all-hex mesh results, and the explicit time step of mixed degenerate meshes is no worse than 25% less than the critical time step on an all-hex mesh. All of the mixed degenerate meshes perform vastly superior to all-tet mesh. All of the degenerate mesh elements were as robust as the hex and tet elements and showed no tendency towards instability or inversion even at very large deformation levels.

CONCLUSIONS

Running the standard hex element computations on a wide variety of degenerate element connectives appears to be a viable computational strategy. Computational results on mixed degenerate meshes appeared to be first order complete, convergent, stable, and relatively efficent. Pursuit of meshing algorithms that mesh the majority of the domain with hex elements while allowing use of a variety of degenerate hex elements as needed to facilitate meshing appears to be a fruitful endeavor.

SANDIA NATIONAL LABORATORIES

Sandia National Laboratories is a multi-program laboratory managed and operated by Sandia Corporation, a wholly owned subsidiary of Lockheed Martin Corporation, for the U.S. Department of Energy's National Nuclear Security Administration under contract DE-AC04-94AL85000.

ACKNOWLEDGMENT

The authors would also like to acknowledge the following members of the Sierra/SolidMechanics development team: XXX.

REFERENCES

[1] Staten, M. L., Owen, S. J., and Blacker, T. D., 2005. "Unconstrained paving and plastering: A new idea for all hexahedral mesh generation". In Proceedings of the 14th International Meshing Roundtable, pp. 399–416.

[2] Shimada, K., 2011. "Current issues and trends in meshing and geometric processing for computational engineering analysis". *Journal of Computing and Information Science in Engineering,* ***11***.

[3] Shepherd, J. F., and Johnson, C. R., 2008. "Hexahedral mesh generation constraints". *Engineering with Computers,* ***24***, pp. 195–213.

[4] Yamakawa, S., and Shimada, K., 2003. "Fully-automated hex-dominant mesh generation with directionality control via packing rectangular solid cells". *International Journal for Numerical Methods in Engineering,* ***57***, pp. 2099–2129.

[5] Flanagan, D. P., and Belytschko, T., 1981. "A uniform strain hexahedron and quadrilateral with orthogonal hourglass control". *International Journal for Numerical Methods in Engineering,* ***17***, pp. 679–706.

[6] SIERRA Solid Mechanics Team, 2011. Sierra/SolidMechanics 4.22 user's guide. SAND Report 2011-7597, Sandia National Laboratories, Albuquerque, NM and Livermore, CA.

[7] SIERRA Solid Mechanics Team, 2013. Sierra/SM verification tests manual. SAND Report 20XX-XXXX, Sandia National Laboratories, Albuquerque, NM and Livermore, CA.

[8] Cox, J. V., 2012. Manufactured solutions for testing sierra/sm a potential path toward testing finite deformation and contact capabilities. SAND Memorandum 20XX-XXXX, Sandia National Laboratories, Albuquerque, NM and Livermore, CA.